Synthesis, characterization and catalytic oxidation of carbon monoxide over cobalt oxide

Hung-Kuan Lin[a,b], Hui-Chi Chiu[b], Hsin-Chi Tsai[a,b], Shu-Hua Chien[b,c,*], and Chen-Bin Wang[a,**]

[a]*Department of Applied Chemistry, Chung Cheng Institute of Technology, National Defense University, Tahsi, Taoyuan, 33509, Taiwan, Republic of China*

[b]*Institute of Chemistry, Academia Sinica, Taipei, 11529 Taiwan, Republic of China*

[c]*Department of Chemistry, National Taiwan University, Taipei, 10764, Taiwan, Republic of China*

Received 14 January 2003; accepted 27th March 2003

A mix-valenced cobalt oxide, CoO_x, was prepared from cobalt nitrate aqueous solution through a precipitation with sodium hydroxide and an oxidation by hydrogen peroxide. Further, other pure cobalt oxide species were refined from the CoO_x by temperature-programmed reduction (TPR) at 170, 230 and 300 °C (labeled as R-170, R-230 and R-300, respectively). They were characterized by X-ray (XRD), infrared (IR), thermogravimetry (TG) and TPR. The major composition of CoO_x is CoO(OH), with a small amount of Co^{4+} species; R-170 is CoO(OH) with a hexagonal structure; R-230 is Co_3O_4 with a spinel structure and R-300 is CoO with a cubic structure. Their catalytic activities toward the CO oxidation were further studied in a continuous flow microreactor. The results indicated that the relative activity decreased significantly with the oxidation state of cobalt, *i.e.*, CoO (+2) $\gtrsim$ Co_3O_4 (+8/3) $\gg$ CoO(OH) (+3) $\gtrsim$ CoO_x (> +3).

KEY WORDS: cobalt oxide; TPR; CO oxidation.

1. Introduction

Metal oxides are widely used in the field of heterogeneous catalysis. Cobalt oxide is one of the versatile materials among the transition metal oxides. Unsupported cobalt oxide is an active catalyst in air pollution control for abatement of CO [1–5], NO_x [6–8] and organic pollutants from effluent streams [9,10]. Also, cobalt oxide is important in the development of the rechargeable battery [11–13] and the CO sensor [3,14–16].

It is known that Co_3O_4 and CoO are the stable oxides in the cobalt oxide system [17,18], while the valence of cobalt higher than +3 is thermally unstable. Some literatures [19–22] reported the special methods to obtain higher valence cobalt oxides, such as Co_2O_3 and CoO_2. However, these methods always end up with either a mixture of CoO and Co_2O_3 or a mixture of Co_2O_3 and CoO_2.

In order to have better control in the preparation of high-valence cobalt oxide and pure cobalt oxides, in the present paper, we adopted the precipitation–oxidation method with hydrogen peroxide as the oxidant. A series of pure cobalt oxide species were further refined from the high-valence cobalt oxide by the TPR technique. Characterization of these oxides includes XRD, TG/DTG, TPR and IR. Their catalytic activities toward CO oxidation were further studied in a continuous flow microreactor.

* Corresponding authors. E-mail: chiensh@gate.sinica.edu.tw
** Corresponding author. E-mail: chenbin@ccit.edu.tw

2. Experimental

2.1. Sample preparation

The crude cobalt oxide (marked as CoO_x) with a high valence state of cobalt was synthesized by the precipitation–oxidation method in an aqueous solution. The precipitation process was carried out at 50 °C with 50 ml of 0.6 M $Co(NO_3)_2 \cdot H_2O$ solution added drop by drop to 100 ml of 3.2 M NaOH solution; 100 ml of H_2O_2 (50 wt%) was then introduced drop by drop under constant stirring. Using the H_2O_2 as an oxidizing agent, instead of NaOCl [22], avoids possible chloride ion contamination. The precipitate was then filtered, washed with deionized distilled water and dried in an oven at 110 °C for 20 h. The dried product was ground and preserved in a desiccator as fresh samples.

2.2. Techniques of characterization

Thermal gravimetry analysis (TG/DTG) was carried out using a Seiko TG/DTA 300 system. The rate of heating was maintained at 10 °C min^{-1} and the mass of the sample was ~10 mg. The measurement was carried from RT to 1000 °C under nitrogen flowing at the rate of 100 ml min^{-1}.

1011-372X/03/0600–0169/0

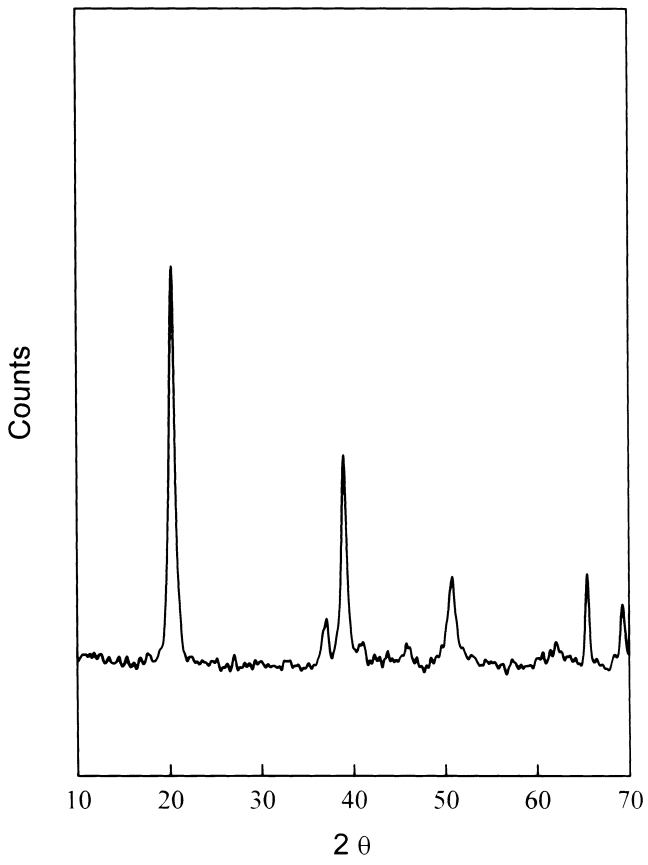

Figure 1. The XRD spectrum of CoO_x.

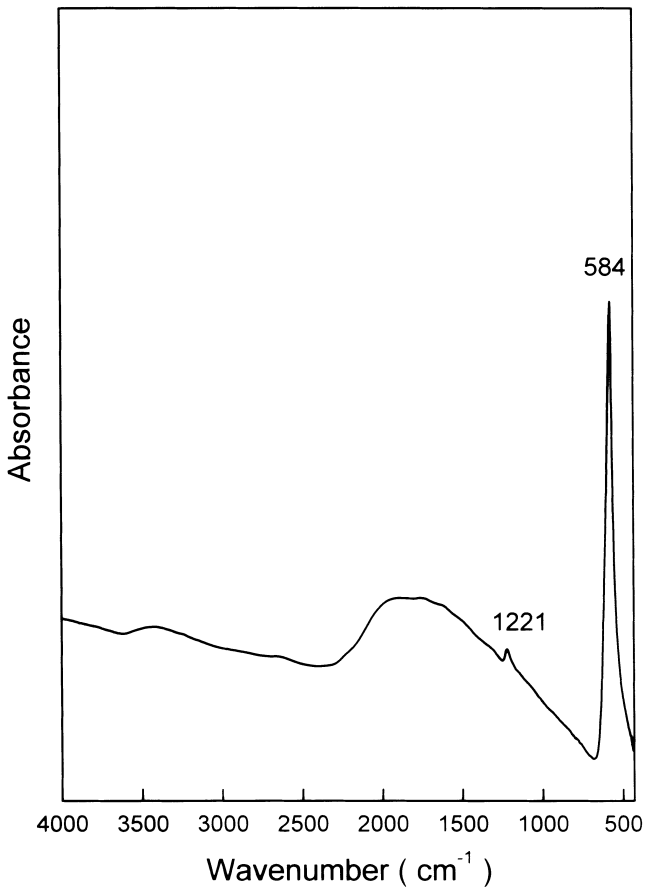

Figure 2. The IR spectrum of CoO_x.

TPR of cobalt oxides was performed using 10% H_2 in Ar as the reducing gas. The gas flow rate was adjusted by mass flow controller under 25 ml min^{-1}. The cell used for TPR was a quartz tube of inner diameter 8 mm, and 80 mg of the catalyst was mounted on quartz wool. The hydrogen consumption in the experiment was monitored by a thermal conductivity detector (TCD) on raising the sample temperature from RT to 500 °C at a constant rate of 5 °C min^{-1}.

The XRD analyses of the samples were carried out using a Siemens D5000 diffractometer. The patterns were run with a Ni-filtered Cu $K_{\alpha 1}$ radiation ($\lambda =$ 1.5405 Å).

IR spectra of samples were obtained by a Bomen DA-8 spectrometer in the range of 500 to 4000 cm^{-1}. One milligram of each powder sample was diluted with 200 mg of vacuum-dried IR-grade KBr powder and subjected to a pressure of 8 tons.

2.3. Activity test

The catalytic activity of prepared samples toward CO oxidation was carried out in a continuous-flow micro-reactor. A 25-ml min^{-1} stream of reactant gas (mixed 10% O_2/He with 4% CO/He) was catalyzed with 40 mg of freshly prepared catalysts. The reactor temperature was raised stepwise from room temperature to 200 °C. The reaction products were analyzed on-line using a Varian 3700 gas chromatograph with a carbosphere column. Before reaction, the catalyst was pretreated in flowing 10% O_2/He at 110 °C for 1 h to drive away molecules preadsorbed from the atmosphere.

3. Results and discussion

3.1. Characterization of the prepared high valence cobalt oxide—CoO_x

Figure 1 shows XRD pattern of CoO_x. It indicates that the pattern matches the JCPDS 14-0673 file identifying cobalt oxyhydroxide, CoO(OH), with hexagonal structure. The infrared spectrum of CoO_x is shown in figure 2. The spectrum displays one distinct band at 584 cm^{-1} that originated by the stretching vibration of the metal–oxygen bond [23]. The presence of this band indicates that cobalt is situated in an oxygen octahedral environment in the hexagonal structure. In addition to the stretching vibration of the metal–oxygen bond, an extremely broad, diffuse band centered around 1800 cm^{-1} is attributed to the hydrogen-stretching vibrations into the interlayer space and the band at 1221 cm^{-1} is the hydrogen-bending vibration [24].

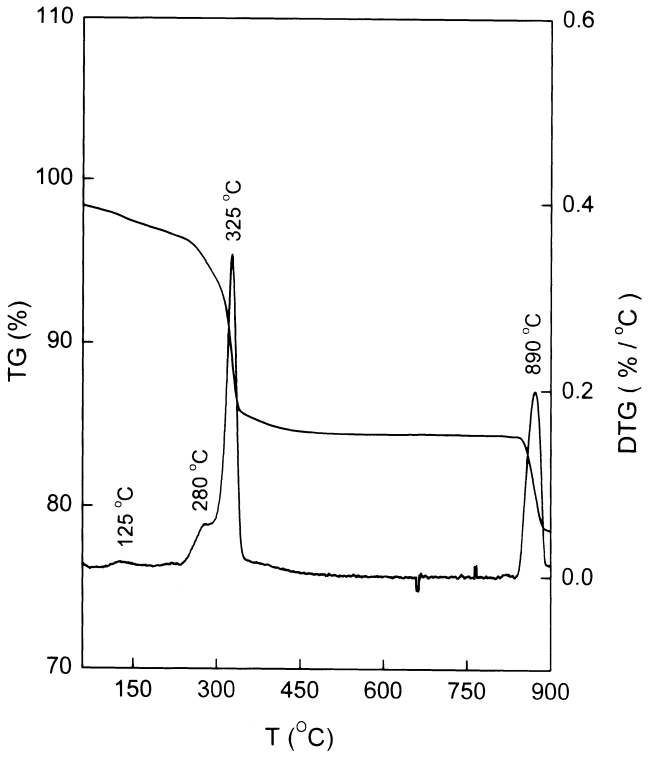

Figure 3. The TG/DTG profiles of CoO_x in a dynamic nitrogen environment.

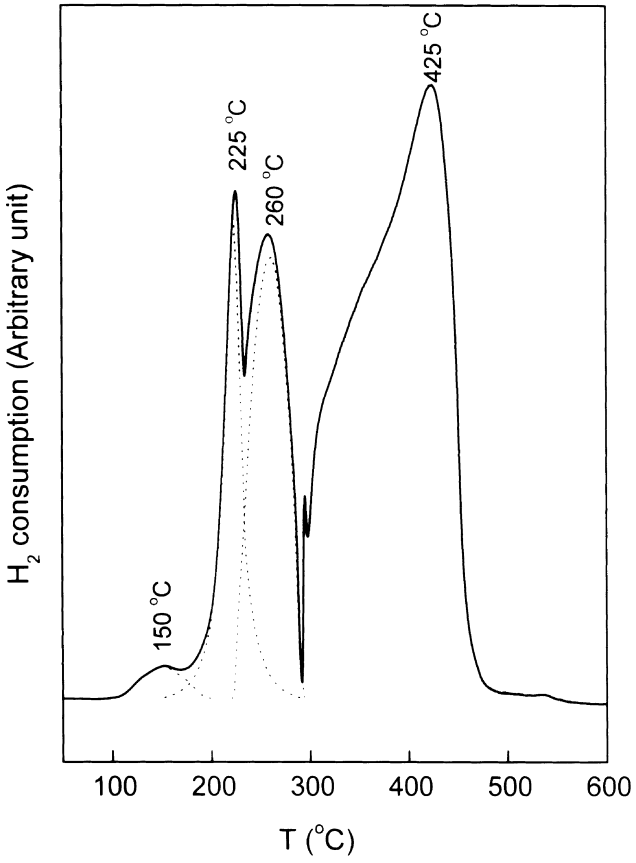

Figure 4. The TPR profile of CoO_x.

Figure 3 shows the TG/DTG curves for the decomposition of CoO_x in a dynamic nitrogen (100 ml min^{-1}) environment. The TG curve shows the three weight loss steps and the DTG curve shows the maximum loss rate at 280, 325 and 890 °C (labeled as T_1, T_2 and T_3), respectively. Prior to 280 °C, the tardy weight loss should have come from the desorption of water on the CoO_x surface in the heating process. Weight loss of 3.6% in T_1 step is mainly the decomposition of CoO_2 into CoO(OH) according to equation (1) (theoretical weight loss is 16%).

$$4\,CoO_2 \cdot H_2O \rightarrow 4\,CoO(OH) + O_2 + 2\,H_2O \quad (1)$$

$$12\,CoO(OH) \rightarrow 4\,Co_3O_4 + O_2 + 6\,H_2O \quad (2)$$

$$2\,Co_3O_4 \rightarrow 6\,CoO + O_2 \quad (3)$$

Obviously, only a little amount of CoO_2 exists. Weight loss of 10.5% in T_2 step should be decomposed of CoO(OH) into Co_3O_4 according to equation (2) (theoretical weight loss is 12.7%). Weight loss of 6.4% in T_3 step is the decomposition of Co_3O_4 into CoO according to equation (3) that is close to the theoretical value (6.6%). Therefore, the CoO_x is suggested that contains CoO(OH), CoO_2, and occluded water.

Figure 4 shows the TPR profile of CoO_x. The reductive signals (labeled as R_1, R_2, R_3 and R_4) of CoO_x in TPR proceed in four consecutive steps at 150, 225, 260 and 425 °C, respectively. A comparison of these TPR traces with TG/DTG in figure 3 reveals that the peaks can be assigned to CoO_2, CoO(OH), Co_3O_4 and CoO species for R_1, R_2, R_3 and R_4, respectively. The CoO_2 is initially reduced to CoO(OH), and then subsequently reduced to Co_3O_4, CoO and Co. Accordingly, the following four successive steps are designated in TPR on raising the sample temperature.

$$2\,CoO_2 \cdot H_2O + H_2 \rightarrow 2\,CoO(OH) + 2\,H_2O \quad (4)$$

$$6\,CoO(OH) + H_2 \rightarrow 2\,Co_3O_4 + 4\,H_2O \quad (5)$$

$$Co_3O_4 + H_2 \rightarrow 3\,CoO + H_2O \quad (6)$$

$$CoO + H_2 \rightarrow Co + H_2O \quad (7)$$

The ratio of each cobalt oxide species in CoO_x is quantitatively determined from the consumption of hydrogen in TPR traces. By means of deconvolution, the relative area (dashed lines) of R_1, R_2, R_3 and R_4 are 0.20, 1.0, 1.8 and 6.4, respectively. Comparison with the theoretical values (3, 1, 2 and 6, respectively) that are based on equations (4) to (7) also proved that the CoO_x consists of a little amount of CoO_2.

3.2. Characterization of cobalt oxide derivatives

In order to prepare and characterize pure cobalt oxides, three oxide derivatives—CoO(OH), Co_3O_4 and CoO from CoO_x are prepared by controlled hydrogen reduction in TPR to 170, 230 and 300 °C [labeled as R-170, R-230 and R-300], respectively.

Figure 5 presents XRD patterns for cobalt oxide derivatives. The results show that CoO_x and R-170 samples are similar to each other. Both CoO_x and R-170 [CoO(OH)] are hexagonal structures. From the XRD pattern, it is clear that CoO_x undergoes changes in its composition and structure up to a reduction temperature above 230 °C. R-230 sample converts into a spinel structure [Co_3O_4] and R-300 sample has a face-centered cubic (fcc) structure [CoO].

Figure 6 displays TPR profiles of a series of cobalt oxide derivatives. Slight variations exhibit the reductive property of those species. Except for the R_1 peak at 150 °C, the TPR of the R-170 sample is very similar to that of the CoO_x sample. The disappearance of R_1 peak in R-170 sample proves that a pure CoO(OH) species exists at 170 °C reduction. Also, the disappearance of R_1 and R_2 peaks in R-230 sample proves that a pure Co_3O_4 species exists at 230 °C reduction. R-300 sample shows only a single peak at 425 °C. This peak is therefore assigned to the reduction of CoO.

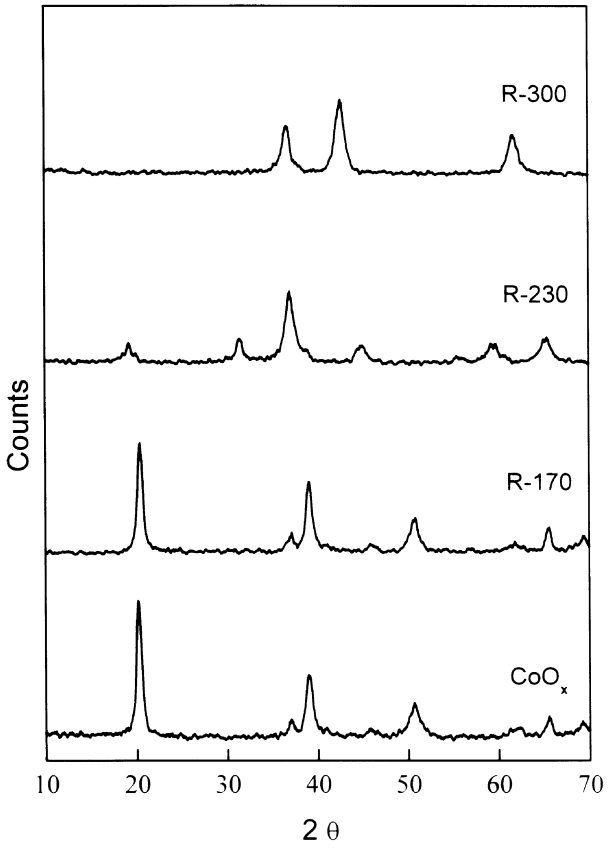

Figure 5. XRD characterization for a series of cobalt oxide derivatives.

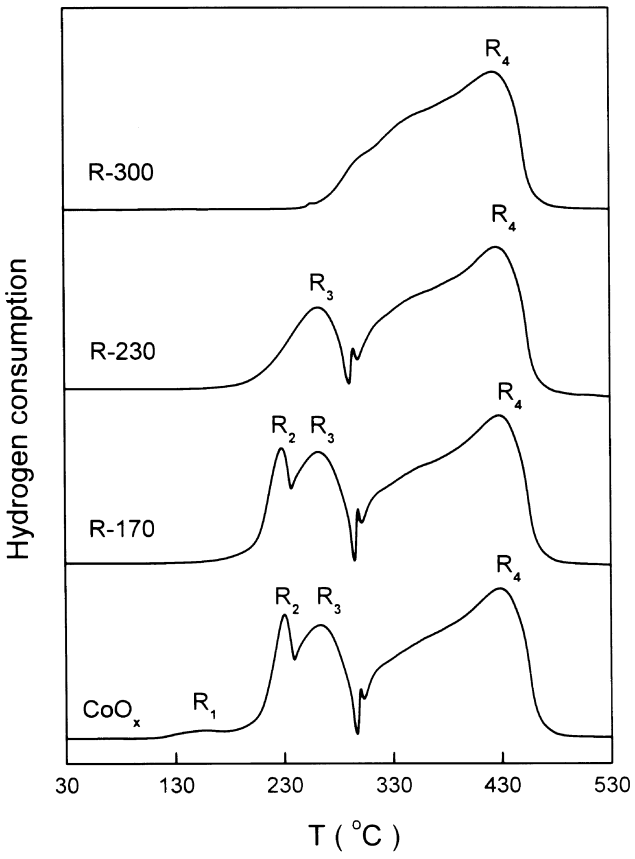

Figure 6. TPR characterization for a series of cobalt oxide derivatives.

In order to understand the crystallographic sites occupation and the cationic jumps along the phase transition of cobalt oxides, the IR absorption spectra are measured for a series of cobalt oxide derivatives. Figure 7 shows the absorption spectra of individual oxides pretreated under various conditions. The IR spectrum of R-230 displays 2 distinct and sharp bands at 574 (ν_1) and 665 (ν_2) cm^{-1} that originated by the stretching vibrations of the metal–oxygen bond [23,25]. The ν_1 band is characteristic of OB_3 (where B denotes the Co^{3+} in the octahedral hole) vibration and the ν_2 band is attributed to the ABO_3 (where A denotes the Co^{2+} in the tetrahedral hole) vibration in the spinel lattice [22]. In a comparison of the hexagonal structure [CoO(OH) and CoO_x] with the spinel structure (Co_3O_4), only one distinct band at 584 cm^{-1} is observed instead of ν_1 and ν_2. The band at 584 cm^{-1} is similar to the OB_3 vibration in the spinel lattice of Co_3O_4, but it has been displaced by 10 cm^{-1} into the higher frequency. Obviously, the displacement of the band is in accordance with the structure. For the face-centered cubic structure of CoO, two bands are observed that may be a mixture of Co_3O_4 and CoO. These results suggest that on reduction of the CoO_x sample at temperatures above 230 °C, a part of the octahedral oriented cobalt ions jump into tetrahedral coordination along a phase transition.

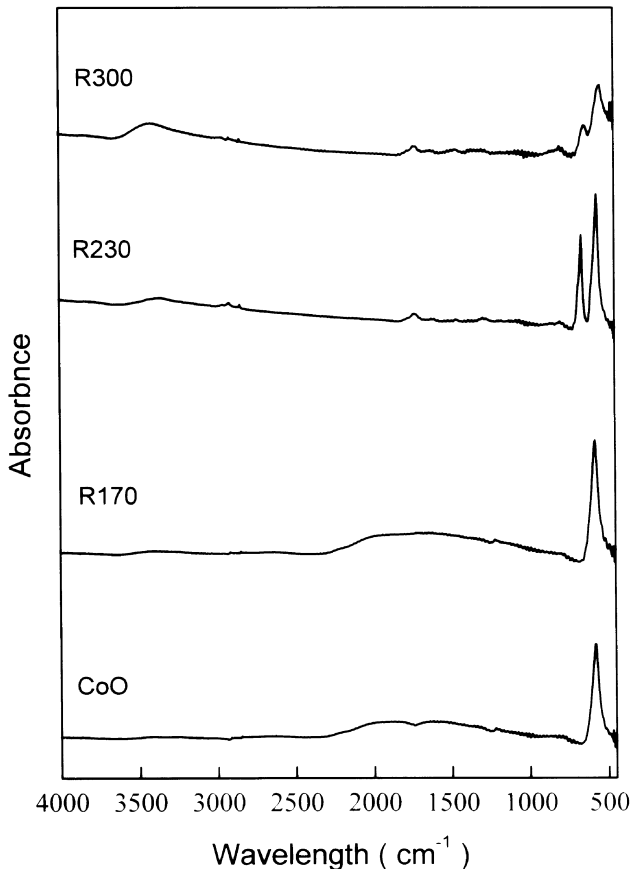

Figure 7. FTIR characterization for a series of cobalt oxide derivatives.

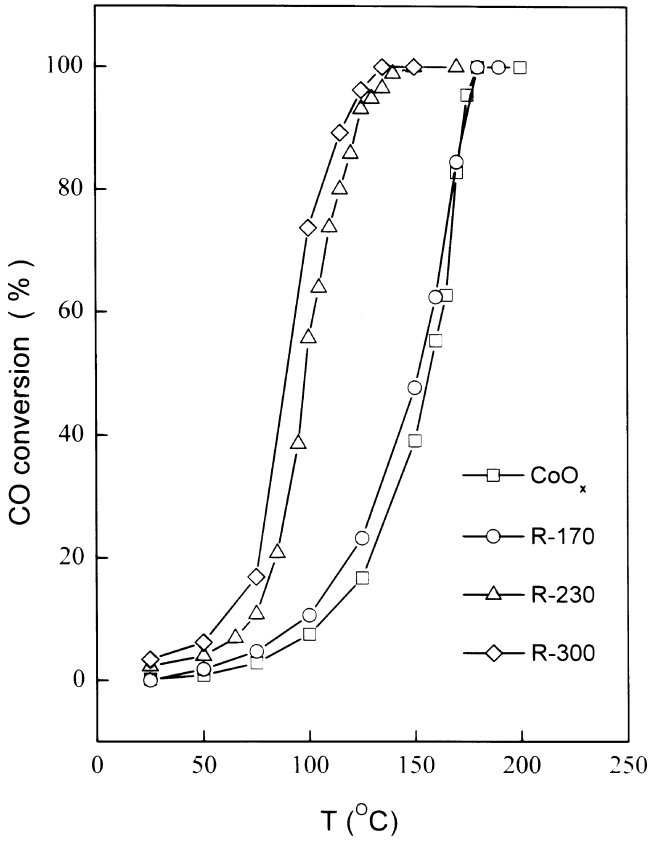

Figure 8. Conversion profiles for CO oxidation over cobalt oxides.

In addition to the stretching vibrations of the metal–oxygen bond, the broad and diffuse absorption hump spreading from ca. 1000 to 2300 cm^{-1} is attributed to hydrogen vibrations into the interlayer space. This observation, together with the XRD patterns, unambiguously shows that the phase of CoO_x and R-170 samples is actually a CoO(OH) phase.

3.3. Catalytic activities toward the CO oxidation

Figure 8 compares the CO conversion obtained from CoO_x and oxide derivatives catalysts in activity tests. The CO conversion over each fresh catalyst generally increased with the reaction temperature. Conceivably, the observed T_{50} (the conversion of CO reached 50%) decreased significantly with the oxidation state of cobalt, that is, CoO (+2) $\gtrsim$ Co_3O_4 (+8/3) $\gg$ CoO(OH) (+3) $\gtrsim$ CoO_x (> +3). The best active catalysts are achieved over the high temperature reduction (both R-230 and R-300), where T_{50} is reached at temperatures as low as 100 °C and full conversion is reached at about 130 °C, while the least active catalysts are obtained by the low temperature reduction (R-170) and crude cobalt oxide, where T_{50} is reached around 150 °C and full conversion is reached at about 180 °C.

The catalysts via the high temperature reductive treatment for R-300 and R-230 may produce some specific sites of defects that increase the tendency to adsorb gas molecules and promote the activity. The increase in T_{50} for R-170 and CoO_x may be caused by the OH group in the hexagonal structure that affects the tendency to adsorb gas molecules and decreases the CO oxidation activity. In a previous paper [26], we proposed two mechanisms for CO/O_2 co-adsorption over CoO_x and oxide derivatives' catalysts. In the absence of lattice oxygen, the weakly adsorbed CO on CoO_x and R-170 has to be oxidized by the weakly bonded active oxygen, while the lattice oxygen on R-230 and R-300 is more active for CO oxidation. Apparently, the variation of T_{50} with the cobalt oxides' catalysts suggests that the structure and the oxidation state of cobalt play an important role in their activity toward CO oxidation.

4. Conclusion

A mixed cobalt oxide, CoO_x, was prepared by precipitation–oxidation method and further refined other pure cobalt oxide with a controlled hydrogen reduction. Based on the characterizations and the catalytic activities toward the CO oxidation of cobalt

oxides, we propose

(1) the decomposition of CoO_x under N_2 proceeded in three consecutive steps, *i.e.*,

$$CoO_x \xrightarrow{T_d \sim 270\,^\circ C} CoO(OH) \xrightarrow{T_d \sim 310\,^\circ C} Co_3O_4 \xrightarrow{T_d \sim 870\,^\circ C} CoO$$

(2) the reduction of CoO_x in TPR proceeded in four consecutive steps, *i.e.*,

$$CoO_x \xrightarrow{T_r \sim 160\,^\circ C} CoO(OH) \xrightarrow{T_r \sim 230\,^\circ C} Co_3O_4$$

$$\xrightarrow{T_r \sim 260\,^\circ C} CoO \xrightarrow{T_r \sim 430\,^\circ C} Co$$

(3) the catalytic activities toward the CO oxidation were decreased significantly with the oxidation state of cobalt, *i.e.*, $CoO(+2) \gtrsim Co_3O_4(+8/3) \gg CoO(OH)(+3) \gtrsim CoO_x(> +3)$.

Acknowledgment

The authors acknowledge the financial support for this study by the National Science Council of the Republic of China.

References

[1] Y.J. Mergler, A. van Aalst, J. van Delft and B.E. Nieuwenhuys, J. Catal. 161 (1996) 310.
[2] Y.J. Mergler, A. van Aalst, J. van Delft and B.E. Nieuwenhuys, Appl. Catal. B10 (1996) 245.
[3] K. Omata, T. Takada, S. Kasahara and M. Yamada, Appl. Catal. A146 (1996) 255.
[4] Y.J. Mergler, J. Hoebink and B.E. Nieuwenhuys, J. Catal. 167 (1997) 305.
[5] J. Jansson, J. Catal. 194 (2000) 55.
[6] H. Hamada, Y. Kintaichi, M. Inaba, M. Tabata, T. Yoshinari and H. Tsuchida, Catal. Today 29 (1996) 53.
[7] A. Torncrona, M. Skoglundh, P. Thormahlen, E. Fridell and E. Jobson, Appl. Catal. B14 (1997) 131.
[8] D. Pietrogiacomi, S. Tuti, M.C. Campa and V. Indovina, Appl. Catal. B28 (2000) 43.
[9] E. Garbowski, M. Guenin, M.C. Marion and M. Primet, Appl. Catal. 64 (1990) 209.
[10] A.S.K. Sinha and V. Shankar, J. Chem. Eng. Biochem. Eng. 52 (1993) 115.
[11] F. Lichtenberg and K. Kleinsorgen, J. Power Sources 62 (1996) 207.
[12] E. Antolini and E. Zhecheva, Mater. Lett. 35 (1998) 380.
[13] T.J. Boyle, D. Ingersoll, T.M. Alam, C.J. Tafoya, M.A. Rodriguez, K. Vanheusden and D.H. Doughty, Chem. Mater. 10 (1998) 2770.
[14] H. Yamaura, J. Tamaki, K. Moriya, N. Miura and N. Yamazoe, J. Electrochem. Soc. 144 (1997) L158.
[15] H. Yamaura, K. Moriya, N. Miura and N. Yamazoe, Sens. Actuators B65 (2000) 39.
[16] E. Gulari, C. Güldür, S. Srivannavit and S. Osuwan, Appl. Catal. A182 (1999) 147.
[17] D.R. Lide, *Handbook of Chemistry and Physics*, 72nd ed. (1991–1992). CRC Press.
[18] R.B. King, *Encyclopedia of Inorganic Chemistry*, Vol. 2 (John Wiley & Sons, 1994).
[19] R. Van Zee, Y. Hamrick, S. Li and W. Weltner, J. Phys. Chem. 96 (1992) 7247.
[20] M. Elemongy, M. Gouda and Y. Elewady, J. Electroanal. Chem. 76 (1977) 367.
[21] D. Chen, Y. Wen and N.N. Rommel, J. Electrochem. Soc. 131 (1984) 731.
[22] St. G. Christoskova, M. Stoyanova, M. Georgieva and D. Mehandjiev, Mater. Chem. Phys. 60 (1999) 39.
[23] C. Spenser and D. Schroeder, Phys. Rev. B9 (1974) 3658.
[24] R.G. Delaplane, J.A. Ibers, J.R. Ferraro and J. Rush, J. Chem. Phys. 50 (1969) 1921.
[25] T. Andrushkevich, G. Boreskov, V. Popovskii, L. Pliasova, L. Karakchiev and A. Ostankovitch, Kinet. Katal. 6 (1968) 1244.
[26] H.K. Lin, C.B. Wang, H.C. Chiu and S.H. Chien, Catal. Lett. (2002); 86 (2003) 63.